Voxel-based correlation of ^{18}F-THK5351 accumulation with gray matter structural networks in cognitively normal older adults

Yoko Shigemoto (shigemoyk@gmail.com)
National Center of Neurology and Psychiatry https://orcid.org/0000-0003-2524-2498
Daichi Sone
National Center of Neurology and Psychiatry
Norihide Maikusa
National Center of Neurology and Psychiatry: Kokuritsu Seishin Shinkei Center
Yukio Kimura
National Center of Neurology and Psychiatry: Kokuritsu Seishin Shinkei Center
Fumio Suzuki
National Center of Neurology and Psychiatry: Kokuritsu Seishin Shinkei Center
Hiroyuki Fujii
National Center of Neurology and Psychiatry: Kokuritsu Seishin Shinkei Center
Noriko Sato
National Center of Neurology and Psychiatry: Kokuritsu Seishin Shinkei Center
Hiroshi Matsuda
Southern Research Institute: Southern Research

Short communication

Keywords: caudate nucleus, cognitively normal older adult, gray matter, network, neuroinflammation, tau

Posted Date: December 22nd, 2020

DOI: https://doi.org/10.21203/rs.3.rs-132629/v1

Abstract

Background

No previous studies have examined the correlations between tau and gray matter network alterations in cognitively normal (CN) older adults. Here, we investigated the correlations between ^{18}F-THK5351 and local network measures at the voxel level.

Material and methods

We recruited 47 amyloid-negative CN older adults (65.0 ± 7.9 years, 55% women). All participants underwent structural magnetic resonance imaging (MRI) and ^{11}C-Pittsburgh compound-B and ^{18}F-THK5351 positron emission tomography (PET) scans. Single-subject gray matter networks extracted from T1-weighted MRI data based on cortical similarities were analyzed using the graph theoretical approach. The ^{18}F-THK5351 PET and four local network measures (betweenness centrality, clustering coefficient, characteristic path length, and degree) were evaluated to calculate voxel-wise correlations among the imaging modalities.

Result

Significant positive correlations between ^{18}F-THK5351 and local network measures were detected in the bilateral caudate.

Conclusion

Our findings suggest that tau and neuroinflammation in CN older adults may influence local gray matter network in the caudate.

Introduction

Neuropathological studies have revealed that neurofibrillary tangles mainly accumulate in the medial temporal lobe (MTL) with age. We previously detected significant negative voxel-wise correlations between ^{18}F-THK5351 and gray matter (GM) volume in the MTL in cognitively normal (CN) older adults without amyloid β deposits [1].

Graph theoretical analysis allows brain networks to be studied as nodes and edges. In this method, graphs are defined via nodes representing small brain regions and via edges representing connecting regions that have statistically high cortical similarities within single subjects. GM networks based on intracortical similarities derived from three-dimensional (3D) T1-weighted imaging have been proposed

[2], but no studies have as yet examined the correlations between tau accumulation and GM network alterations.

^{18}F-THK5351, one of the first-generation tau tracers, detected tau associated regions in Alzheimer's disease (AD) and considered the promising biomarker for tau [3]. However, because of off-target binding to monoamine oxidase B (MAO-B), ^{18}F-THK5351 does not reflect only tau pathology and is considered to reflect astrogliosis-related neuroinflammation in addition to tau [4]. Considering the key role of neuroinflammation in neurodegeneration [5], ^{18}F-THK5351 may give important information on tau and neuroinflammation.

In this study, we used ^{18}F-THK5351 PET and GM network to investigate the associations of tau and inflammatory pathology with local structural network measures in amyloid-negative CN older adults.

Materials And Methods

Participants

We recruited 47 CN older adults from the Brain Mapping by Integrated Neurotechnologies for Disease Studies (Brain/MINDS) project (grant number 18dm0207017h0005). All individuals underwent structural magnetic resonance imaging (MRI) and ^{11}C-Pittsburgh compound-B (PiB) and ^{18}F-THK5351 positron emission tomography (PET) scans, as well as cognitive testing that included the Mini-Mental State Examination (MMSE), global Clinical Dementia Rating Scale (CDR), and Wechsler Memory Scale-Revised Logical Memory II (WMSR LM-II). The inclusion criteria were as follows: visually negative ^{11}C-PiB PET results, a global CDR score of 0, an MMSE score of $\geq$ 26, performance within education-adjusted norms for the WMSR LM-II, no neurological or psychiatric disorders, and no medications that affect cognition. Amyloid negativity was visually assessed by a board-certified nuclear medicine specialist from ^{11}C-PiB PET.

Image acquisition

All participants underwent structural MRI scans on a Siemens 3-T scanner (Verio; Siemens, Erlangen, Germany) to obtain 3D sagittal T1-weighted magnetization-prepared rapid acquisition with gradient echo (MPRAGE) images (repetition time/echo time, 1.900/2.52 ms; 1.0-mm effective slice thickness with no gap; 300 slices; matrix, 256 × 256; field of view, 25 × 25 cm; acquisition time; 4 min 18 s).

All PET/computed tomography (CT) scans were acquired using a Siemens/Biograph TruePoint16 Scanner (3D acquisition mode; 81 image planes; 16.2-cm axial field of view; 4.2-mm transaxial resolution; 4.7-mm axial resolution; 2-mm slice interval). Low-dose CT scans for attenuation correction were performed prior to the PET scans. ^{11}C-PiB PET scans were acquired as dynamic scans in LIST mode 50-70 min after a bolus injection of 555 ± 185 MBq of ^{11}C-PiB. ^{18}F-THK5351 scans were acquired as dynamic scans in LIST mode 40–60 min after a bolus injection of 185 ± 37 MBq of ^{18}F-THK5351.

PET/CT data were reconstructed using an iterative 3D ordered subset expectation maximization reconstruction algorithm. All MRI and PET data were acquired in the same manner as in previous studies [1, 6].

MRI and PET processing

GM images were segmented from 3D T1-weighted images using Statistical Parametric Mapping Software version 12 (SPM12; Functional Imaging Laboratory, University College London, London, UK) implemented in MATLAB 7.12. Partial volume-corrected ^{11}C-PiB and ^{18}F-THK5351 PET images obtained using PETPVE12 toolbox [7] were normalized using SPM12. Each participant's PET images were coregistered to the corresponding T1-weighted images and normalized to the Montreal Neurological Institute (MNI) space with the Diffeomorphic Anatomical Registration Through Exponentiated Lie (DARTEL) method [8]. After spatial normalization, the standardized uptake value ratio (SUVR) for ^{11}C-PiB and ^{18}F-THK5351 PET images were calculated using the individual's positive mean uptake value of cerebellar GM as the reference region. Finally, each SUVR of PET image was smoothed using an 8-mm full width at half maximum (FWHM) Gaussian kernel. MRI and PET data were processed in the same manner as in previous studies [1, 6].

Single-subject GM networks

We resliced all native segmented GM images into 2 × 2 × 2-mm isovoxels to standardize voxel sizes and reduce dimensionality. Single-subject GM networks were extracted based on intracortical similarity from native space GM segmentations using a previously described fully automated method (https://github.com/bettytijms/Single_Subject_Grey_Matter_Networks; version 20150902) [2]. Nodes were defined as small regions of interest in the brain (3 × 3 × 3 voxel cubes, corresponding to 6 × 6 × 6 mm^3). Connectivity was defined by high statistical similarities quantified with Pearson's correlations across the GM density values of corresponding voxels between any two nodes. Then, each node was rotated by a θ angle at multiples of 45° and reflected over all axes to identify the maximal similarity value with the target node. To construct unweighted and undirected graphs, the GM similarity matrices were binarized after determining a threshold. The threshold for each graph was determined using false discovery rate technique to correct for multiple comparisons which is based on the random permutation method to ensure similar chance to include average 5% spurious correlations for all subjects [9]. The following four local network measures were calculated: betweenness centrality (i.e., the proportion of the shortest paths that run through a node), clustering coefficient (i.e., the level of interconnectedness of neighboring nodes), characteristic path length (i.e., the shortest distance between two nodes), and degree (i.e., the number of edges per node).

To compare each participant's local network measures at the cubic level, we superimposed the images on the corresponding resliced GM of the MNI space. For single-subject GM networks, each participant's local network measure images were smoothed using a 10-mm FWHM Gaussian kernel in the same manner as

in the previous study [10]. This value (10 mm) was determined by nearly doubling the resolution of one side of a cube (6 mm).

Voxel-wise correlations between ^{18}F-THK5351 PET and GM network

To evaluate relationships between ^{18}F-THK5351 and local network measures, we used the Biological Parametric Mapping (BPM) toolbox [11]. The toolbox allows voxel-wise correlations across two imaging modalities based on the general linear model. We analyzed the correlations between ^{18}F-THK5351 and four local network measures (betweenness centrality, clustering coefficient, characteristic path length, and degree). The results with the following criteria were deemed significant: a height threshold of $p < .05$ (family-wise error [FWE] corrected) with an extent threshold of 100 voxels.

Results

Participants' demographics are shown in Table 1. Mean age ± standard deviation was 65.0 ± 7.9 years and 26 of the participants (55%) were women. Mean cognitive scores were 0.0 ± 0.2 for the CDR sum of boxes, 29.3 ± 1.1 for the MMSE, and 13.4 ± 2.9 for the WMSR LM-II.

Table 1
Participants' demographics

	Cognitively normal older adults
No. (% women)	47 (26)
Age, yr	65.0 ± 7.9 [50–86]
Education, yr	14.3 ± 2.4 [9–22]
MMSE	29.3 ± 1.1 [26–30]
WMSR LM-II	13.4 ± 2.9 [8–19]

Values are mean ± standard deviation [range]. MMSE, Mini-Mental State Examination; WMSR LM-II, Wechsler Memory Scale-Revised Logical Memory II.

^{18}F-THK5351 showed cerebral accumulation mainly in the MTL and, to a lesser extent, in the inferior temporal lobe, insula, posterior cingulate/precuneus, and basal frontal lobe (Fig. 1). In addition, elevated ^{18}F-THK5351 accumulation was observed in the caudate nucleus, putamen, and thalamus.

We found significant positive correlations between ^{18}F-THK5351 and four local network measures in the bilateral caudate (Table 2, Fig. 2). No significant negative correlations were detected.

Table 2

Clusters of positive correlations between ^{18}F-THK5351 accumulation and local network measures detected by voxel-wise correlation analysis using biological parametric mapping.

	Cluster size (no. of voxels)	*Z*-value (peak voxel)	Talairach coordinates (*x, y, z*)	Location of peak voxels	
Betweenness centrality	432	Inf	8, 14, 14	Rt	Caudate
Clustering coefficient	313	6.98	−6, 6, 13	Lt	Caudate
Characteristic path length	357	7.06	−6, 6, 13	Lt	Caudate
Degree	505	7.57	−4, 6, 11	Lt	Caudate
Results were family-wise error-corrected for multiple comparisons ($p < .05$) with an extent					
threshold of 100 voxels. Lt, left; Rt, right.					
Note that these are the nearest gray matter of peak voxels.					

Discussion

This is the first study to investigate the direct voxel-wise imaging correlations between ^{18}F-THK5351 and local network measures in amyloid-negative CN older adults. We found positive correlations of ^{18}F-THK5351 with local GM network measures in the bilateral caudate. These finding suggests that tau and inflammatory pathology in CN older adults may influence local gray matter network in the caudate.

We found cerebral ^{18}F-THK5351 accumulation mainly in the MTL and, to a lesser extent, in the inferior temporal lobe, insula, posterior cingulate/precuneus, and basal frontal lobe. These findings correspond to Braak stage III – IV and are considered to reflect primary age-related tauopathy (PART) [12]. In addition, elevated ^{18}F-THK5351 accumulation was observed in the caudate nucleus, putamen, and thalamus, which was considered to be largely due to non-specific binding to MAO-B [13].

The similarity-based GM networks obtained using graph theoretical analysis allow the evaluation of structural networks at local level. We visualized these local network measures at voxel level, enabling direct comparisons across images. The BPM analysis revealed significant voxel-wise positive correlations of ^{18}F-THK5351 with four local network measures in the caudate. Betweenness centrality is the proportion of the shortest paths that run through a node and our findings suggest that the caudate plays an important role as a hub. The increase of clustering coefficient indicates the progress of segregation with the ^{18}F-THK5351 accumulation. Whereas, the increase of characteristic path length suggests the

decrease of the local efficiency in the caudate. Thus, although caudate is overactivated as a hub, tau and inflammatory pathology also locally disrupts the balance between integration and segregation.

Neuropathological studies have shown that tau pathology accumulates in the caudate nucleus as well as in the MTL in PART patients with higher Braak stages (e.g., III/IV) [14]. In addition, a previous PET study using [^{11}C]L-deprenyl-D2 reported that MAO-B levels in the basal ganglia increase by an average of 8% per decade in healthy individuals [15]. Another study using quantitative enzyme radioautography and in situ hybridization histochemistry also detected high levels of MAO-B in the caudate nucleus [16]. MAO-B levels increase with age and are considered to increase oxidative stress, which may increase the vulnerability of the brain dopamine system to age-related degeneration [17]. A recent structural network study using T1-weighted images in patients with idiopathic rapid eye movement sleep behavior disorder, which often precedes neurodegenerative disease, reported overactivity of the caudate nucleus as a hub, suggesting that such overactivity might be a potential biomarker [18].

Anatomically, the caudate nucleus is connected to the MTL and is part of the cortico-striato-thalamic loops [19, 20]. The caudate plays a critical role in cognitive aging, which includes decreases in the functioning of inhibitory mechanisms, executive control, or planning and cognitive slowing, as measured by increases in response times [21]. Moreover, the caudate seems to be linked to apathy [22], which is the most frequent abnormal behavior before memory deficits become noticeable in AD. A recent systematic review and meta-analysis reported that apathy was associated with an approximately 2-fold increased risk of dementia in memory clinic patients, indicating that apathy might be one of the useful indicators of prodromal dementia [23]. Several MRI studies have detected reductions in caudate volume with aging [24, 25], which is consistent with previous autopsy data indicating an estimated 15% decrease in caudate volume from ages 25 to 75 years [26]. These atrophies may be secondary to the accumulation of tau and inflammatory pathology in the caudate. Because the caudate is connected to the MTL, our findings of overactivity as well as local network disruption in the caudate may be induced by tau and neuroinflammation in the MTL, which is the first brain region to be affected by tau pathology with aging.

This study has several limitations. First, the relatively small number of participants. Second, the high affinity of ^{18}F-THK5351 for MAO-B in the basal ganglia and thalamus may mask the network alterations in the MTL. Third, we have not conducted correlation analysis of networks using other modalities such as resting-state functional MRI or diffusion tensor imaging. To date, no studies have examined the correlation of functional MRI and GM network analysis. The interaction analysis is needed to clarify the inter-modality correlations and understand the pathophysiology of network alterations in CN older adults. Fourth, we found some of the peak voxels were contained inside the lateral ventricles adjust to caudate. This reduced accuracy of anatomical registration might be possibly caused by using large 6 mm cube voxels, which is necessary for keeping the 3D structure of the cortex intact.

Conclusion

We found voxel-wise positive correlations between ^{18}F-THK5351 and local network measures in the caudate. These results suggest that tau and inflammatory pathology may influence local gray matter network of the caudate in CN older adults.

Abbreviations

BPM: Biological Parametric Mapping; CDR: Clinical Dementia Rating; FWHM: Full width at half maximum; GM: Gray matter; MAO-B: Monoamine oxidase B; MMSE: Mini-Mental State Examination; MTL: Medial temporal lobe; PART: Primary age-related tauopathy; PiB: Pittsburgh compound-B; SPM: Statistical Parametric Mapping; SUVR: Standardized uptake value ratio; WMSR LM-II: Wechsler Memory Scale-Revised Logical Memory II

Declarations

Ethics approval and consent to participate

All procedures performed in studies involving human participants were in accordance with the ethical standards of the institutional and/or national research committee and with the 1964 Helsinki declaration and its later amendments or comparable ethical standards.

All participants gave written informed consent to participate in the study, which was approved by the institutional ethics committee at the National Center of Neurology and Psychiatry (A2014-146).

Consent for publication

Not applicable.

Availability of data and material

The datasets used and analyzed during the current study are available from the corresponding author on reasonable request.

Competing interests

The authors declare that they have no competing interests.

Funding

This study was supported by the following funding sources: the Brain Mapping by Integrated Neurotechnologies for Disease Studies (Brain/MINDS) project (grant no. 18dm0207017h0005), the Japan Agency for Medical Research and Development (AMED); and an Intramural Research Grant (30-10) for Neurological and Psychiatric Disorders from the National Center of Neurology and Psychiatry (Japan).

Authors' contributions

YS and HM designed the study, performed the analysis. DS and HM collected the data and carried out the experiments. NM gave technical support. YK, FS, and HF participated in the data investigation. YS wrote the manuscript. HM and NS revised the manuscript. All authors read and approved the final manuscript.

Acknowledgements

We would like to thank Mr. Tetsuro Ono of Dainippon Printing Co., Ltd., for valuable suggestions regarding individual network analyses. We also thank all imaging technicians who contributed to the study.

References

1. Shigemoto Y, Sone D, Ota M, Maikusa N, Ogawa M, Okita K, et al. Voxel-based correlation of ^{18}F-THK5351 accumulation and gray matter volume in the brain of cognitively normal older adults. EJNMMI Res. 2019;9:81. doi: 10.1186/s13550-019-0552-3.
2. Tijms BM, Seriès P, Willshaw DJ, Lawrie SM. Similarity-based extraction of individual networks from gray matter MRI scans. Cereb Cortex. 2012;22:1530-41. doi: 10.1093/cercor/bhr221.
3. Betthauser TJ, Lao PJ, Murali D, Barnhart TE, Furumoto S, Okamura N, et al. In Vivo Comparison of Tau Radioligands ^{18}F-THK-5351 and ^{18}F-THK-5317. J Nucl Med. 2017;58:996-1002. doi: 10.2967/jnumed.116.182980.
4. Okamura N, Harada R, Ishiki A, Kikuchi A, Nakamura T, Kudo Y. The development and validation of tau PET tracers: current status and future directions. Clin Transl Imaging. 2018;6:305-16. doi: 10.1007/s40336-018-0290-y.
5. Calsolaro V, Edison P. Neuroinflammation in Alzheimer's disease: Current evidence and future directions. Alzheimers Dement. 2016;12:719-32. doi: 10.1016/j.jalz.2016.02.010.
6. Shigemoto Y, Sone D, Imabayashi E, Maikusa N, Okamura N, Furumoto S, et al. Dissociation of Tau Deposits and Brain Atrophy in Early Alzheimer's Disease: A Combined Positron Emission Tomography/Magnetic Resonance Imaging Study. Front Aging Neurosci. 2018;10:223. doi: 10.3389/fnagi.2018.00223.
7. Gonzalez-Escamilla G, Lange C, Teipel S, Buchert R, Grothe MJ, Alzheimer's Disease Neuroimaging Initiative. PETPVE12: an SPM toolbox for Partial Volume Effects correction in brain PET - Application to amyloid imaging with AV45-PET. 2017;147:669-77. doi: 10.1016/j.neuroimage.2016.12.077.
8. Ashburner J. A fast diffeomorphic image registration algorithm. NeuroImage. 2007;38:95-113. doi: 10.1016/j.neuroimage.2007.07.007.
9. Noble WS. How does multiple testing correction work? Nat Biotechnol. 2009;27:1135-7. doi: 10.1038/nbt1209-1135.
10. Fujii H, Sato W, Kimura Y, Matsuda H, Ota M, Maikusa N, et al. Altered Structural Brain Networks Related to Adrenergic/Muscarinic Receptor Autoantibodies in Chronic Fatigue Syndrome. J Neuroimaging. 2020 doi: org/10.1111/jon.12751

11. Casanova R, Srikanth R, Baer A, Laurienti PJ, Burdette JH, Hayasaka S, et al. Biological parametric mapping: A statistical toolbox for multimodality brain image analysis. 2007;34:137-43. doi: 10.1016/j.neuroimage.2006.09.011.
12. Crary JF, Trojanowski JQ, Schneider JA, Abisambra JF, Abner EL, Alafuzoff I, et al. Primary age-related tauopathy (PART): a common pathology associated with human aging. Acta Neuropathol. 2014;128:755-66. doi: 10.1007/s00401-014-1349-0
13. Ng KP, Pascoal TA, Mathotaarachchi S, Therriault J, Kang MS, Shin M, et al. Monoamine oxidase B inhibitor, selegiline, reduces 18F-THK5351 uptake in the human brain. Alzheimers Res Ther. 2017;9:25. doi: 10.1186/s13195-017-0253-y.
14. Zhu K, Wang X, Sun B, Wu J, Lu H, Zhang X, et al. Primary Age-Related Tauopathy in Human Subcortical Nuclei. Front Neurosci. 2019;13:529. doi: 10.3389/fnins.2019.00529.
15. Fowler JS, Volkow ND, Wang GJ, Logan J, Pappas N, Shea C, et al. Age-related increases in brain monoamine oxidase B in living healthy human subjects. Neurobiol Aging. 1997;18:431-35. doi: 10.1016/s0197-4580(97)00037-7
16. Saura J, Bleuel Z, Ulrich J, Mendelowitsch A, Chen K, Shih JC, et al. Molecular neuroanatomy of human monoamine oxidases A and B revealed by quantitative enzyme radioautography and in situ hybridization histochemistry. 1996;70:755-74. doi: 10.1016/s0306-4522(96)83013-2.
17. Cohen G. Monoamine oxidase and oxidative stress at dopaminergic synapses. J Neural Transm Suppl. 1990;32:229-38. doi: 10.1007/978-3-7091-9113-2_33.
18. Park KM, Lee HJ, Lee BI, Kim SE. Alterations of the brain network in idiopathic rapid eye movement sleep behavior disorder: structural connectivity analysis. Sleep Breath. 2019;23:587-93. doi: 10.1007/s11325-018-1737-0.
19. Deweer B, Lehéricy S, Pillon B, Baulac M, Chiras J, Marsault C, et al. Memory disorders in probable Alzheimer's disease: the role of hippocampal atrophy as shown with MRI. J Neurol Neurosurg Psychiatry. 1995;58:590-7. doi: 10.1136/jnnp.58.5.590.
20. Brück A, Portin R, Lindell A, Laihinen A, Bergman J, Haaparanta M, et al. Positron emission tomography shows that impaired frontal lobe functioning in Parkinson's disease is related to dopaminergic hypofunction in the caudate nucleus. Neurosci Lett. 2001;311:81-4. doi: 1016/s0304-3940(01)02124-3.
21. Hicks LH, Birren JE. Aging, brain damage, and psychomotor slowing. Psychological Bulletin. 1970;74:377-96. doi: 10.1037/h0033064.
22. Bruen PD, McGeown WJ, Shanks MF, Venneri A. Neuroanatomical correlates of neuropsychiatric symptoms in Alzheimer's disease. Brain. 2008;131:2455-63. doi: 10.1093/brain/awn151.
23. van Dalen JW, van Wanrooij LL, van Charante EPM, Brayne C, van Gool WA, Richard E. Association of Apathy With Risk of Incident Dementia: A Systematic Review and Meta-analysis. JAMA Psychiatry. 2018;75:1012-21. doi: 10.1001/jamapsychiatry.2018.1877.
24. Jernigan TL, Archibald SL, Fennema-Notestine C, Gamst AC, Stout J, Bonner J, et al. Effects of age on tissues and regions of the cerebrum and cerebellum. Neurobiol Aging. 2001;22:581-94. doi:

10.1016/s0197-4580(01)00217-2.

25. Raz N, Rodrigue KM, Kennedy KM, Head D, Gunning-Dixon F, Acker JD. Differential aging of the human striatum: longitudinal evidence. AJNR Am J Neuroradiol. 2003;24:1849-56.
26. Eggers R, Haug H, Fischer D. Preliminary report on macroscopic age changes in the human prosencephalon: A stereologic investigation. Journal fuer Hirnforschung. 1984;25:129-39.

Figures

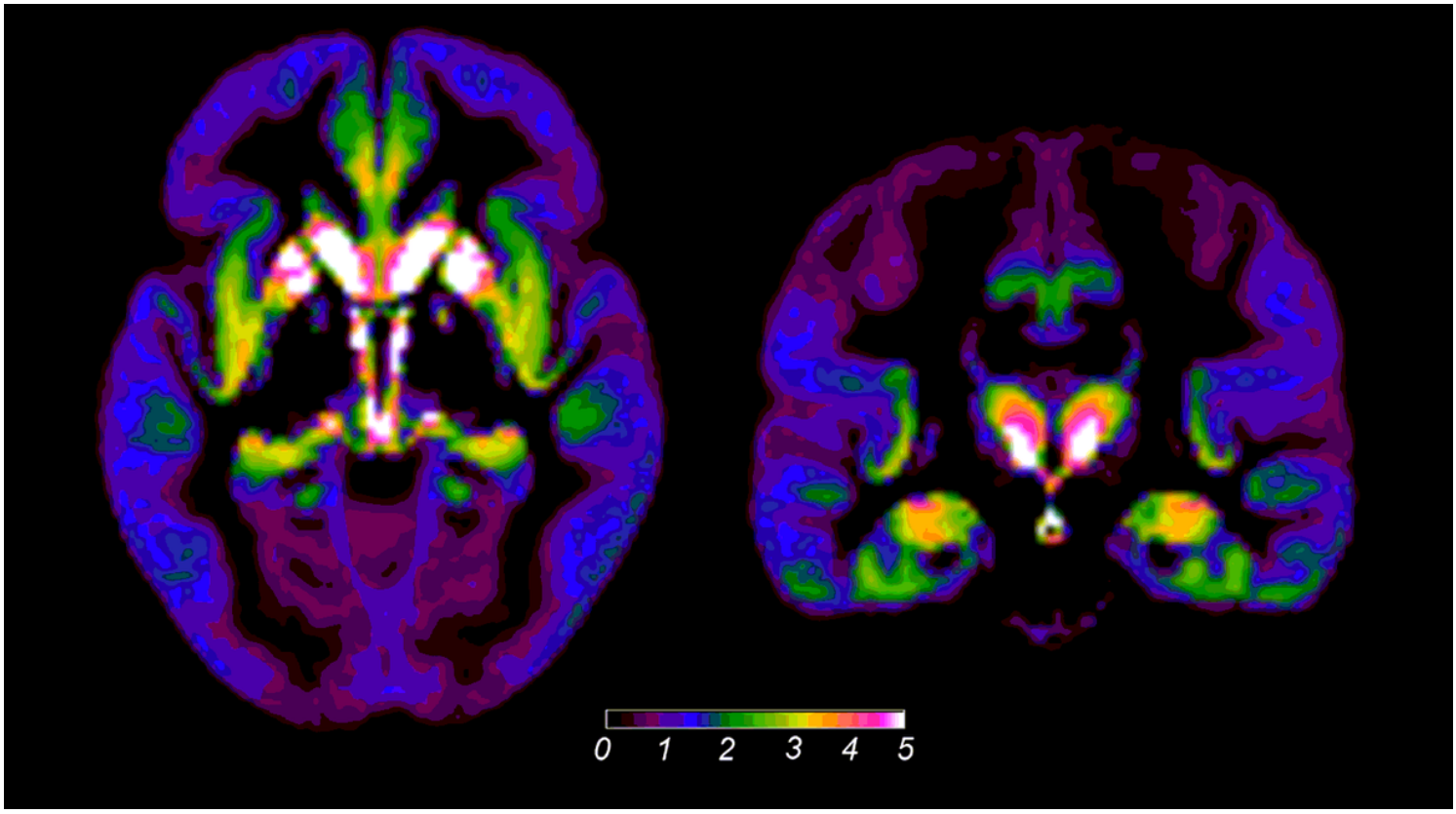

Figure 1

Mean SUVR images of 18F-THK5351 in cognitively normal older adults. SUVR, standardized uptake value ratio.

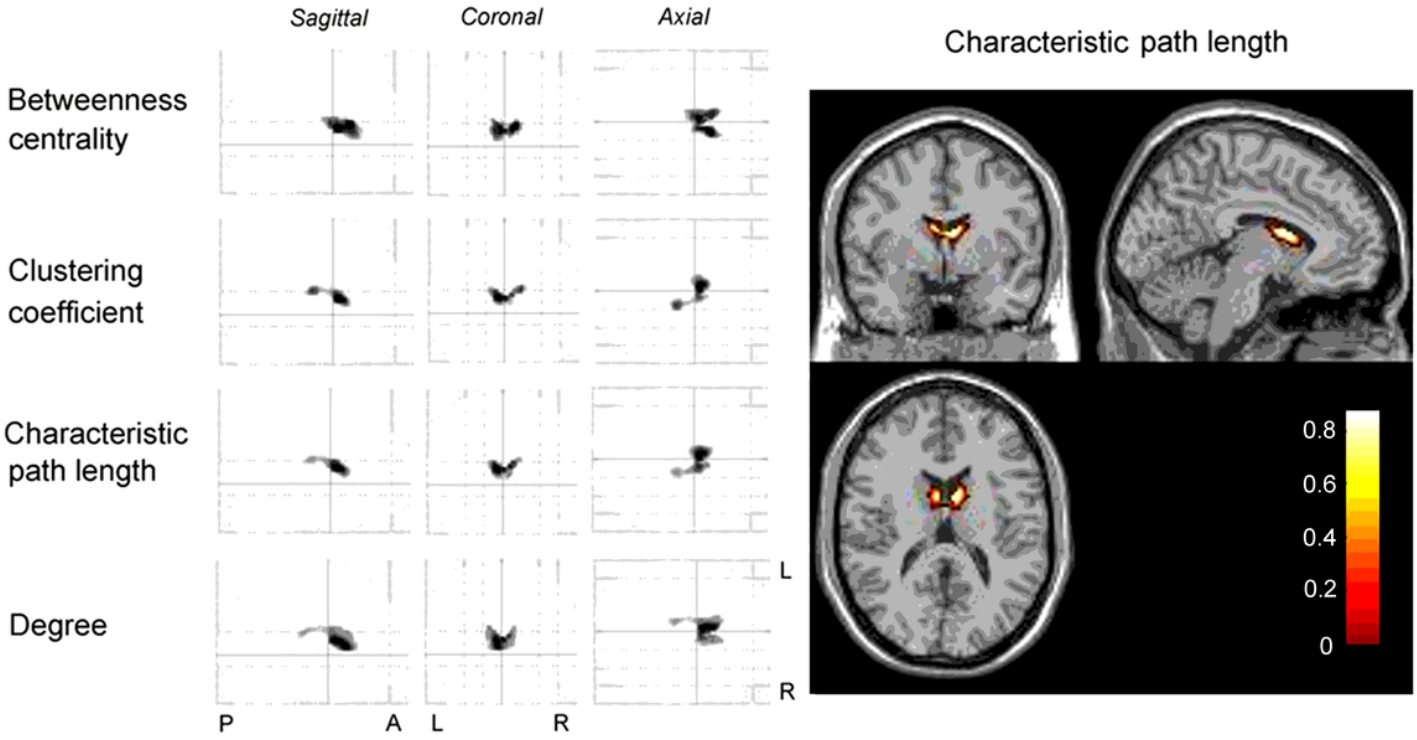

Figure 2

Voxel-wise correlations between 18F-THK5351 and four local network measures in cognitively normal older adults. Significant positive correlations between 18F-THK5351 and local network measures were detected in the bilateral caudate (FWE corrected p<.05 with a 100-voxel extent threshold). A, anterior; L, left; P, posterior; R, right.